Effects of pyrolysis conditions on Miscanthus and corncob chars: Characterization by IR, solid state NMR and BPCA analysis

Budai, Alice ; Calucci, Lucia ; Rasse, Daniel P ; Strand, Line Tau ; Pengerud, Annelene ; Wiedemeier, Daniel B ; Abiven, Samuel ; Forte, Claudia

Abstract: Infrared and 13C solid state nuclear magnetic resonance spectroscopies and benzene polycarboxylic acids (BPCA) analysis were used to characterize the structural changes occurring during slow pyrolysis of corncob and Miscanthus at different temperatures from 235 °C to 800 °C. In the case of corncob, a char sample obtained from flash carbonization was also investigated. Spectroscopic techniques gave detailed information on the transformations of the different biomass components, whereas BPCA analysis allowed the amount of aromatic structures present in the different chars and the degree of aromatic condensation to be determined. The results showed that above 500 °C both corncob and Miscanthus give polyaromatic solid residues with similar degree of aromatic condensation but with differences in the structure. On the other hand, at lower temperatures, char composition was observed to depend on the different cellulose/hemicellulose/lignin ratios in the feedstocks. Flash carbonization was found to mainly affect the degree of aromatic condensation.

DOI: https://doi.org/10.1016/j.jaap.2017.09.017

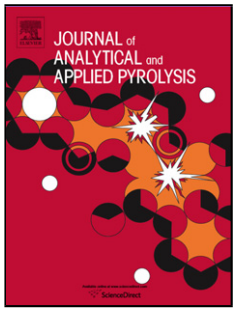

Title: Effects of pyrolysis conditions on *Miscanthus* and corncob chars: characterization by IR, solid state NMR and BPCA analysis

Authors: Alice Budai, Lucia Calucci, Daniel P. Rasse, Line Tau Strand, Annelene Pengerud, Daniel Wiedemeier, Samuel Abiven, Claudia Forte

PII: S0165-2370(17)30477-1
DOI: http://dx.doi.org/10.1016/j.jaap.2017.09.017
Reference: JAAP 4144

To appear in: *J. Anal. Appl. Pyrolysis*

Received date: 26-5-2017
Revised date: 6-9-2017
Accepted date: 18-9-2017

Please cite this article as: Alice Budai, Lucia Calucci, Daniel P.Rasse, Line Tau Strand, Annelene Pengerud, Daniel Wiedemeier, Samuel Abiven, Claudia Forte, Effects of pyrolysis conditions on Miscanthus and corncob chars: characterization by IR, solid state NMR and BPCA analysis, Journal of Analytical and Applied Pyrolysishttp://dx.doi.org/10.1016/j.jaap.2017.09.017

Effects of pyrolysis conditions on *Miscanthus* and corncob chars: characterization by IR, solid state NMR and BPCA analysis

Alice Budai[a,b], Lucia Calucci[c], Daniel P. Rasse[a], Line Tau Strand[b], Annelene Pengerud[d], Daniel Wiedemeier[e], Samuel Abiven[e], Claudia Forte[c*]

[a]Department of Soil Quality and Climate Change, Norwegian Institute of Bioeconomy Research, Høgskoleveien 7, 1430 Ås, Norway

[b]Faculty of Environmental Sciences and Natural Resource Management, Norwegian University of Life Science, P.O. Box 5003, N-1433 Ås NORWAY

[c]Istituto di Chimica dei Composti OrganoMetallici, CNR, via G. Moruzzi 1, 56124 Pisa, Italy

[d]Norconsult AS, Jåttåflaten 27, 4020 Stavanger, Norway

[e]Department of Geography, University of Zurich, Winterthurerstr. 190, CH-8057 Zurich, Switzerland

*Corresponding Author: claudia.forte@cnr.it

Highlights

- A multi-method approach is mandatory for obtaining detailed information on char structure
- Lignin/hemicellulose/cellulose ratio in biomass affects pyrolysis behavior
- The condensed aromatic architecture of chars depends on feedstock type
- Flash carbonization favors the formation of condensed aromatic structures

Abstract

Infrared and ^{13}C solid state nuclear magnetic resonance spectroscopies and benzene polycarboxylic acids (BPCA) analysis were used to characterize the structural changes occurring during slow pyrolysis of corncob and *Miscanthus* at different temperatures from 235 °C to 800 °C. In the case of corncob, a char sample obtained from flash carbonization was also investigated. Spectroscopic techniques gave detailed information on the transformations of the different biomass components, whereas BPCA analysis allowed the amount of aromatic structures present in the different chars and their degree of condensation to be determined. The results showed that above 500 °C both corncob and *Miscanthus* give polyaromatic solid residues with similar degree of aromatic condensation but with differences in the structure. On the other hand, at lower temperatures, char composition was observed to depend on the different cellulose/hemicellulose/lignin ratios in the feedstocks. Flash carbonization was found to mainly affect the degree of aromatic condensation.

Keywords: biomass; biochar; solid state nuclear magnetic resonance; infrared spectroscopy; benzene polycarboxylic acids; char structure; aromaticity

1. Introduction

Biomass is a valuable resource that is receiving growing attention thanks to its great potential in relation to renewable energy production and environmental issues. Biomass is currently utilized in thermochemical processes for the production of biofuels; in this process char is also produced, which can be considered as highly valuable "green" carbon. The conversion of biomass into char to be used as soil amendment represents *per se* an efficient carbon sequestration method while at the same time improving soil fertility [1]. Biomass-derived char can also be combusted for heat and power or used for applications in several crucial fields, such as water purification, catalysis, electronics, and biomedicine [2,3].

Different technologies can be used to produce carbonized organic matter, i.e. slow and fast pyrolysis, gasification, hydrothermal carbonization, and flash carbonization [3,4]. The pyrolysis treatment induces successive chemical reactions of biomass with increasing temperature, i.e. dehydration, decarboxylation, and polymerization, which cause a progressive loss of hydrogen and oxygen and a related enrichment in carbon, with an increase in aromatic groups and eventually the condensation into aromatic clusters. In particular,

two different aromatic phases are typically distinguished, i.e. an amorphous phase with randomly organized aromatic rings and a crystalline phase constituted by polyaromatic sheets [5]. These molecular scale alterations also cause changes in bulk properties, such as surface area, cation exchange capacity, electrical conductivity, magnetic susceptibility, and crystallinity [6].

The structure of char produced by pyrolysis strongly depends on process parameters, such as the energy supply rate, highest treatment temperature (HTT) reached, pressure, and carrier gas composition [7]. HTT in particular has great influence on the chemical nature of chars, which may vary from slightly charred biomass, when produced at temperatures as low as 200°C, to highly aromatic chars at temperatures up to 800 ^{o}C and beyond [8]. Thus, the potential applications of the resulting char can be quite different, depending on the chemical and physical properties of the feedstock, the method, and the treatment conditions used. For example, the production temperature determines the surface properties of chars (e.g. surface area, pH and cation exchange capacity) [9], relevant for the use of char as soil conditioner, as well as the aromaticity and degree of aromatic condensation, which determine the stability of char against degradation in the environment [10], with implications for the carbon cycle [11]. Hence, a detailed knowledge of the structure of char is important for its use in soils. Due to the growing concern for climate change and the need to mitigate greenhouse gases, several research groups have recently responded to the challenge of understanding the relationship between the properties of chars obtained from biomass and the process conditions used to produce them [12]. To this end, different instrumental techniques and analytical methods have been applied in order to obtain a more thorough physico-chemical characterization of chars, as, for example, ^{13}C solid state Nuclear Magnetic Resonance (SS-NMR) spectroscopy [13] and NMR relaxometry [14], pyrolysis-GC/MS [15], and benzene polycarboxylic acids (BPCA) analysis [16].

The overall purpose of this study was to characterize the structure of chars obtained from two different biomass materials, i.e. *Miscanthus* and corncob, produced by slow pyrolysis with different HTT values and, in the case of corncob, also by flash carbonization. Both types of biomass examined have great potential for useful char production: *Miscanthus* is a high-yielding crop requiring minimal soil preparation, while corncob is an agricultural residue. Infrared (IR) and ^{13}C SS-NMR spectroscopies, two valuable complementary methods

for a qualitative and quantitative investigation of the functional groups present in chars, were used. In particular, ^{13}C SS-NMR allows the aromatization degree as well as the size of the aromatic clusters to be estimated [17,18,19,20,21,22]. Information on the degree of aromatic condensation was also obtained from elemental [23] and BPCA [22,24,25] analyses, the latter allowing the relative contribution of individual molecular markers that reflect the size of the aromatic clusters to be assessed. The combined application of these techniques to the different char samples gave clear indication of the reactions that take place during pyrolysis of corncob and *Miscanthus* and highlighted structural differences between chars obtained from the two biomass materials under the same process conditions.

2. Materials and methods

2.1. Samples

Feedstocks and biochars from a previous study [9] were used. Two carbonization methods were considered, i.e. slow pyrolysis and flash carbonization. Slow pyrolysis was applied to chaffed biomass of grass (*Miscanthus giganteus*) and corncob from maize (*Zea mays*) grown in Serbia (ZP Maize Hybrid 505); flash carbonization was performed on a batch of corncobs from Waimanalo Farm in Hawaii.

In the case of slow pyrolysis the feedstock was prepared as described elsewhere [9]. Target temperatures ranged from 250 to 800 °C and the heating rate was 2.5 °C min^{-1}. Heat supply from the furnace was stopped upon attainment of the set temperature, and the sample was allowed to cool slowly to room temperature. Since exothermic reactions occurred between 250 and 400 °C, the HTT values, resulting from the average of the four thermocouples, were actually higher than the set temperatures.

Flash carbonization was performed according to the method of Antal et al. [26]. The reaction was carried out at 600 °C and lasted 20 min in a vessel pressurized with air, as described in detail elsewhere [9].

All samples were crushed through a 2 mm sieve, ground for greater homogeneity with a ball mill for 3 min at 20 s^{-1} shaking frequency (MM 200, Retsch GmbH, Haan, Germany), and then stored in airtight bags.

2.2. Infrared Reflectance Spectroscopy

Mid-infrared spectra were recorded using a Nicolet iS10 FT-IR spectrometer (Thermo Fisher Scientific Inc., Madison, WI, USA) using diamond attenuated total reflectance (ATR) spectroscopy. Before analysis, each sample was finely ground for two minutes using an agate mortar and then dried at 105 °C to avoid unsystematic influence of possible residual water. After drying, the samples were placed in a desiccator until analysis. 50 mg sample was transferred to the sample holder plate and gently compressed with a spatula to achieve a smooth surface. All samples were analysed in 5 replicates over the spectral range 4000-600 cm^{-1}, with spectral resolution of 4 cm^{-1} and 32 scans per replicate. For the samples produced at the highest temperatures 64 scans per replicate were used.

After baseline correction, performed by Global Parametric Time Warping in R within the PTW package [27,28], the spectra were analysed by deconvolution of the following regions: the saturated (SAT) region from 2980 to 2820 cm^{-1} corresponding to the aliphatic C-H stretching vibration; the unsaturated region from 1800 to 1525 cm^{-1} corresponding to C=O and aromatic C=C bonds; the polysaccharide region from 1185 to 915 cm^{-1} corresponding to O-Alkyl C; the aromatic CH (aroCH) region from 855 to 740 cm^{-1}. The unsaturated region was further divided into the contributions from C=O (1800-1700 cm^{-1}) and from C=C (1650-1525 cm^{-1}). The signal integrals were used to calculate the aromaticity index $AI_{MIR} = I_{C=C}/I_{SAT}$ [29].

2.3. ^{13}C SS-NMR spectroscopy

^{13}C magic angle spinning (MAS) NMR spectra were recorded on a Bruker AMX300WB spectrometer operating at 300.13 MHz for proton and 75.47 MHz for carbon-13, equipped with a 4mm CP-MAS probehead. Both the ^{1}H and ^{13}C 90° pulses were 3.5 µs. Direct excitation (DE) ^{13}C spectra were recorded with proton dipolar decoupling acquiring 4000 scans using a recycle delay of 30 s. ^{1}H-^{13}C cross-polarization (CP) spectra with proton dipolar decoupling were recorded acquiring 4000 scans using a contact time of 2 ms and a recycle delay of 6 s; the RF field strength was 71.5 kHz both for CP and for dipolar decoupling. The experimental parameters were optimized after preliminary tests in order to obtain a higher overall S/N ratio. All spectra were recorded at room temperature with a MAS rate of 8 kHz. The chemical shifts were referenced to TMS using adamantane as external standard. Deconvolution of the spectra was performed using the SPORT-NMR software [30]. The relative signal intensities were used to estimate the contribution of the different

functional groups and components, following the procedure described by Preston et al. [31]. The degree of aromaticity was estimated from the relative signal intensity of aromatic carbons ($AI_{NMR} = I_{aromatic\ C} / I_{total\ C}$) in DE-MAS spectra.

2.4. Electron Paramagnetic Resonance (EPR) spectroscopy

EPR measurements were performed using a Varian (Palo Alto, CA) E112 X-band spectrometer. Spectra were recorded at room temperature using a standard EPR cavity, a microwave power of 1 mW, a time constant of 0.125 s, and a modulation amplitude of 1.25 G. Feedstock and char powders (~20 mg) were inserted in quartz tubes with an internal diameter of 3 mm. Quantification of organic radicals was performed by comparing the double integral of the signal with that of the standard Varian strong pitch measured under identical instrumental conditions [32].

2.5. BPCA analysis

The method of Wiedemeier et al. [16] was applied to milled char and feedstock (Retsch MM301) weighed into quartz tubes in triplicates of 10, 15, and 20 mg. In brief, the samples were digested with 2 mL of 65% HNO_3 for 8 hours at 170 ˚C using sealed pressure chambers (Seif Aufschlusstechnik). The digestates were filtered through ashless grade filter paper (Whatman 589/3) and washed with Millipore water, stopping further digestion by dilution. Aliquots of the resulting samples were passed through cation exchange resin and freeze-dried after collection (CHRIST ALPHA 2-4 LD plus). The freeze-dried samples were re-dissolved in a water/methanol mixture (1:1, v:v) and then passed through a conditioned solid phase extraction column (Supelco Discovery DSC-18, 3 mL tubes, lot:2178501). After drying (Eppendorf Concentrator Plus), the samples were re-dissolved in water for analysis. Chromatographic separation of the BPCAs was carried out according to Wiedemeier et al. [33] using an Agilent 1290 Infinity HPLC system (Santa Clara, U.S.A.) and Agilent Poroshell 120 SB-C18 column (100 mm × 4.6 mm).

BPCAs were in the form of hemimellitic acid and trimellitic acid (B3CA), pyromellitic, mellophanic and prehnitic acids (B4CA), benzene-pentacarboxylic acid (B5CA), and mellitic acid (B6CA). The aromaticity and

aromatic condensation indices were determined as AI_{BPCA} = BPCA/organic C and CI_{BPCA} = B6CA/BPCA, respectively [34].

2.6. Aromatic cluster size calculation

The degree of aromatic condensation was estimated using the rectangle-like polycyclic aromatic ring model presented by Xiao et al. [23]. On the basis of this model, the number of aromatic rings along the two sides of the n×n condensed structure, is related to the atomic ratio H/C through the expression:

$$\frac{H}{C} = \frac{2n+1}{n^2+2n}$$

In the calculations, H/C values resulting from elemental analysis performed in a previous study [9] were used.

This model was here applied also to estimate the degree of aromatic condensation from BPCA analysis data. Assuming a condensed polyaromatic structure with n rings on each of the four sides, the following expression can be easily derived:

$$\frac{B6CA}{BPCA} = \frac{n^2-4n+4}{n^2}$$

The values of n resulting from the calculations were rounded to the nearest integer value.

3. Results

3.1. IR spectroscopy

IR spectra of chars obtained from slow pyrolysis of corncob and *Miscanthus* at different HTT values and of the corncob char obtained through flash carbonization are shown in Figure 1, together with those of feedstocks for comparison. Only negligible differences were observed among the replicates. Band assignment, schematically indicated in the figure, was made according to the literature [6,29], as reported in Table S.1 in the Supporting Information.

Miscanthus and corncob feedstocks showed similar IR spectra, with the typical features of lignocellulosic materials, i.e. peaks due to functional groups in carbohydrates, mainly cellulose and hemicellulose, and lignin

[35]. As can be seen from Figure 1, the spectra are dominated by the broad band at 3600-3320 cm^{-1}, ascribable to the O-H stretching vibrations in hydroxyl and carboxyl groups of lignin and carbohydrates, and the bands in the 1100-1000 cm^{-1} range due to aliphatic C-O-C and alcohol C-O stretching, both ascribable mainly to oxygenated functional groups of cellulose. Typical of lignin are the bands at 1607, 1512, 1248 cm^{-1}, which correspond to aromatic C=C and C-O stretching or bending vibrations, and small bands between 900 to 700 cm^{-1}, ascribable to aromatic C-H deformations. The bands at 1732, 1374, 1203, 1165, 1062, and 1035 cm^{-1} are mainly due to carbohydrates, and in particular to C=O, C-H, C-O-C, and C-O deformation and stretching vibrations of different groups; the bands at 1320 cm^{-1} and 898 cm^{-1} are ascribed to CH_2 rocking and C-H deformation in cellulose, respectively. The band between 3000 and 2800 cm^{-1} is due to C-H stretching vibrations of methylene and methyl groups, and the bands at 1460, 1427, 1335, and 1106 cm^{-1} are ascribed to C-H and C-O deformation, bending, or stretching vibrations of different groups present in both lignin and carbohydrates.

Although a quantitative determination of the different functional groups was not possible due to the absence of a signal that could be used for normalization, comparison of the changes in the relative intensities of the different bands in the spectra of chars obtained in different conditions could be used to highlight compositional variations that take place upon pyrolysis. These changes are highlighted in Figure 2, where the relative intensities of selected spectral contributions, normalized with respect to the total spectral intensity, are shown.

With increasing HTT, we observed the following changes in the spectra typically found during the coalification process [36]: a progressive decrease in the aliphatic hydrogen content above 380 °C, as revealed by examination of the 3000-2800 cm^{-1} band and Figure 2a, the corresponding intensity almost vanishing above 600 °C; an increase in the relative contribution of aromatic structures, up to 500 °C for both corncob and *Miscanthus*, as also highlighted in Figure 2c; a decrease in the relative contribution of carbonyl and carboxyl functional groups in the 1800-1650 cm^{-1} region after an initial increase up to 380 °C (Figure 2d); a decrease in the relative contribution of oxygen containing aliphatic functional groups up to 400 °C for *Miscanthus* and 600 °C for corncob, followed by an increase at higher HTT values (Figure 2e). The 1511 cm^{-1} band, which

represents the C=C stretching vibration of lignin, disappeared for both feedstocks at 400 °C. The spectra also showed an increase in the aromatic CH wags in the 900-700 cm^{-1} region up to 600 °C and then a decrease for higher HTT values, as highlighted in Figure 2f. The OH stretching signal between 3400 and 3300 cm^{-1} steadily decreased with increasing temperature, disappearing above 400 °C. The absence of most bands in the IR spectrum of the char obtained at 800 °C (spectrum not shown) gave evidence of a complete aromatization of the char.

The spectrum of the flash carbonized corncob sample differed from that of the char obtained by slow pyrolysis at a similar temperature (i.e., 600 °C), particularly in the 1250-1000 cm^{-1} region, with a higher aliphatic alcohol content but lower phenolic one, also highlighted in Figure 2e. On the other hand, the flash carbonized sample had similar aromatic content.

Some differences with HTT for the two types of feedstock are worthy of note. In particular, the water O-H band decreased significantly at a lower temperature in the case of corncob; however, the major difference regards the trend of the aliphatic C-O band, which was largely eliminated upon heating already at 380 °C in the case of corncob, whereas it persisted even at the highest HTT values investigated in the case of *Miscanthus*, only gradually decreasing with increasing HTT up to 410 °C and slightly increasing at higher HTT values (Figure 2e). Close examination of the aromatic C-H deformation region (900-700 cm^{-1}) revealed that, for both corncob and *Miscanthus* chars, the signals assigned to isolated hydrogens (870 cm^{-1}) and to two adjacent hydrogens (815 cm^{-1}) were predominant and increased with increasing HTT, whereas the signal corresponding to 3-4 adjacent aromatic protons (750 cm^{-1}) [36] was non-negligible only in the case of corncob and remained practically constant above 480 °C.

3.2. ^{13}C SS-NMR spectroscopy

The ^{13}C DE- and CP-MAS NMR spectra of corncob and *Miscanthus* chars are shown in Figure 3 together with those of the feedstocks for comparison. The trend of the NMR spectra with increasing HTT was similar to that typically observed for carbonized lignocellulosic biomass materials [37,38], with the progressive transformation from a lignocellulosic composition to a highly aromatic structure. The spectral assignment was made following the literature [18,19]; in particular, cellulose signals are in the 60-110 ppm region (C-1

at 104.5 ppm; C-2, C-3, and C-5 at 72.1 and 74.6 ppm, C-4 at 83.3 and 88.1 ppm, and C-6 at 62.2 and 64.5 ppm [39]). These signals are superimposed to hemicellulose signals (C-1 – C-6 carbons) [40] and signals from aliphatic side chains in lignin [41]. The acetate groups of hemicellulose resonate at 21.0 ppm (methyl carbons) and 172.0 ppm (carboxyl carbons) [39]. Apart for the aliphatic side chain signals, lignin also shows signals in the 115-160 ppm region (oxygen-bound aromatic carbons at 147.0, 152.0 and 160.0 ppm; protonated aromatic carbons at 115.4 and 127.0 ppm; aromatic carbons bearing alkyl groups at 133.0 ppm; aromatic carbons ortho and para to oxygen-substituted carbons at 120.0 ppm), a signal at 105.0 ppm due to aromatic carbons of syringyl units, the methoxyl group signal at 55.8 ppm, and the carboxyl carbons signal at 167.2 ppm [41]. The spectrum of *Miscanthus* pyrolysed at 235 °C was similar to that of the feedstock [42]. After pyrolysis at 369 °C, for both *Miscanthus* and corncob, the feedstock signals decreased and broad signals appeared in the aliphatic (0-45 ppm) and in the aromatic (100-155 ppm) spectral regions. The aliphatic signal resulted from the superposition of resonances of both methylene and methyl carbons (∼32 ppm and ∼14 ppm, respectively) formed from the reduction of alkoxy groups [43,44]. The peak maximum shifted from 35 to 12 ppm with increasing HTT; this was ascribed to the increase of non-oxygenated alkyl chains. The aliphatic signal disappeared for HTT values above 400 °C. Carbonyl signals at 205.0 ppm were not detected, even at the lowest treatment temperature, and the carboxyl resonance at 172 ppm was visible only up to 369 °C. Starting at this temperature, the aromatic contribution became dominant with a main peak at 126 ppm, ascribed to unsubstituted aromatic carbons, and two shoulders at 142 and 155 ppm, ascribed to C- and O-substituted aromatic carbons, respectively, probably from original lignins. The latter peak, which tended to disappear for samples treated at the highest HTT values due to loss of oxygen functionality from lignin structures, was mainly from Ar–OH rather than Ar–OCH_3, since no methoxyl signal was observed.

The ^{13}C CP- and DE-MAS spectra of char obtained from flash carbonization of corncob (Figure 3) were very similar to those of slow pyrolyzed corncob at 562 °C, with a relatively broad peak centered at approximately 126 ppm indicating the complete conversion of biomass to aromatic structures.

The relative intensities of the different carbon types obtained from spectral deconvolution of both DE and CP spectra are reported in Table S.2 in the Supporting Information.

Both for *Miscanthus* and corncob treated at high temperatures, the CP process was scarcely effective; this may be due to the lack of protons in highly condensed aromatic structures [37] and/or to a reduction in the proton $T_{1\rho}$ relaxation time caused by the presence of organic free radicals [45,46].

The DE-MAS spectra had the same general features of the CP-MAS spectra but different relative intensities of the signals, with a slightly higher proportion of aromatic carbons; this is due to the generally higher cross-polarization efficiency for alkyl carbons. This considered, notwithstanding the different amount of radical species present in the different samples (see Paragraph 3.3), as well as instrumental factors, both affecting the spectral intensity, for each sample the overall and the relative spectral intensity ascribable to the different components was estimated from the DE-MAS spectra following the procedure suggested by Preston [31]. The results are reported in Table 1. The overall normalized spectral intensity tended to increase with increasing HTT reaching a maximum value at 500-600°C; the decrease observed for higher temperature treatments may be related to the increase in organic radicals, as well as the formation of condensed aromatic structures showing electron conductivity [37], as highlighted by EPR measurements (vide infra). Furthermore, the relative intensities of carbohydrates and lignin signals at different HTT values clearly indicate that the former are degraded at lower temperatures, their contribution becoming very low or undetectable already at 369 °C.

[a] Taken as reference.

3.3. EPR spectroscopy

Miscanthus and corncob feedstocks showed EPR spectra (Figure 4) with a signal typical of organic radicals in amorphous ligno-cellulosic materials [47]. EPR spectra of chars obtained from slow pyrolysis showed the superposition of two signals, one with Lorentzian and the other with Gaussian lineshape, both ascribable to organic radicals. The *g* value, linewidth, and intensity of signals changed with HTT as reported in Table 2. In particular, for HTT values up to 500 °C, a Lorentzian and a Gaussian line with ≈ 4 G and ≈ 8 G linewidth, respectively, were able to reproduce the spectra of all chars. For these chars, the *g* values decreased while the signal intensity, and hence the radical concentration, increased with increasing HTT. The *g* value trend

can be associated to a progressive decrease in the amount of oxygen-containing radical species (e.g. semiquinones) and a concomitant increase in carbon-containing ones (e.g. polyaromatic structures). The radical concentration trend is associated to an increased production of radicals at higher HTT values.

For HTT values above 500 °C, the signal linewidth increased and, as shown in the case of *Miscanthus*, continued to increase with increasing HTT; on the other hand, the radical concentration increased steadily with increasing the temperature up to 600 °C, and decreased at 682 °C. Corncob char produced by slow pyrolysis at 796 °C (not shown) gave a low signal-to-noise EPR signal with a Dyson lineshape typical of conducting materials [48,49].

A more complex spectrum was observed for the corncob char obtained by flash carbonization, which could be well reproduced by a superposition of two Lorentzian and one Gaussian lines (g=2.0026, 2.0024, and 2.0021, ΔHpp = 1.6, 10, and 34 G, and relative contribution of 2, 48, and 50 %, respectively); the overall intensity corresponded to a radical content of (8.1 ± 0.2) 10^{19} spins/g.

3.4. BPCA analysis

BPCAs, obtained by oxidative degradation, were used to infer the relative amount of aromatic moieties of the feedstocks and the pyrolysed samples, as well as their degree of condensation [25,34]. The relative amount of carbon in BPCAs (BPCA-C) and its speciation in benzene-tricarboxylic acids (B3CA), benzene-tetracarboxylic acids (B4CA), benzene-pentacarboxylic acids (B5CA), and benzene-hexacarboxylic acids (B6CA) obtained for the different samples are shown in Figure 5.

The feedstocks had low amounts of BPCA-C (∼ 2%). Slow pyrolysis of *Miscanthus* at HTT = 235 °C resulted in a product having 3.4% detectable BPCA-C, which is comparable to that of the feedstock. However, while for feedstocks B4CA was the predominant component, for the mild pyrolysis product of *Miscanthus* B5CA was preponderant (Figure 5c). In the chars obtained by slow pyrolysis at higher temperatures, BPCA-C was 10 – 20 %, generally increasing with increasing HTT. For these samples comparable amounts of B4-, B5-, and B6CA were determined. After an initial increase, for HTT values higher than 500 °C, B4- and B5CA showed a decrease, whereas B6CA continued to increase. The highest measured contribution of B6CA to the total BPCA

composition (70%) was obtained for the corncob char prepared at 796 °C. The char sample obtained from corncob with flash carbonization showed a total content of biomarkers similar to that obtained by slow pyrolysis at HTT ~ 400 °C, but with a different distribution of BPCA components, and, in particular, a higher amount of B6CA and correspondingly lower amounts of B4- and B5CA.

3.5. Aromatic cluster size estimation

The rectangle-like polycyclic aromatic ring model [23] was applied to estimate the average aromatic cluster size for chars obtained by slow pyrolysis with HTT ≥ 369 °C and for the corncob char obtained by flash carbonization from the H/C atomic ratios and BPCA data, according to the equations reported in paragraph 2.6; the results are shown in Table 3.

The average aromatic cluster sizes determined from H/C and BPCA are in quite good agreement considering that, for HTT < 500 °C, H/C has contributions also from residual proton-rich aliphatic components, whereas, for HTT ≈ 800 °C, B6CA may be underestimated due to incomplete degradation of large polyaromatic clusters. This considered, the following evolution in cluster size with HTT can be envisaged: 4x4, 5x5, and 14x14 clusters formed by slow pyrolysis at HTT < 500 °C, HTT ≤ 600 °C, HTT ≈ 700 °C and HTT ≈ 800 °C, respectively. The char obtained by flash carbonization of corncob was characterized by 7x7 clusters.

4. Discussion

Pyrolysis induces significant changes in the chemical structure of biomass. These generally depend on the type of biomass, the carbonization method as well as the process parameters, as for example HTT. As observed in a previous paper [9] and confirmed by thermogravimetric analysis (TGA; see Figure S.1), during pyrolysis of both corncob and *Miscanthus* most of the mass loss occurred below 400 °C. Moreover, the Van Krevelen diagram relating the atomic ratios H/C and O/C [9] were quite similar for the two types of feedstock and followed the trend typically observed for biomass carbonization processes [5,7,46,50], with an enrichment in carbon and a loss of oxygen and hydrogen in the char. Oxygen was lost more rapidly at temperatures below 450 °C, whereas hydrogen showed a more rapid decrement at higher temperatures.

Spectroscopic data acquired in the present work allowed the processes occurring during pyrolysis to be characterized in detail highlighting the chemical structure of chars produced at different HTT values. In particular, EPR experiments indicated that the reactions occurring during pyrolysis produced organic radicals, the concentration of which strongly increases during the transition from feedstock to char samples (Table 1). The decreasing value of *g* observed for EPR signals by increasing HTT can be associated to a decrease in oxygen atoms and an increase in carbon atoms in the radical species [47]. Below 400 °C, the main changes in the IR spectra (Figure 1) were related to the relative intensities of the O-H and C-O stretching bands which remarkably decreased, particularly in the case of corncob. In agreement with these observations, the ^{13}C SS-NMR spectra showed that the O-alkyl and di-O-alkyl contributions decreased with increasing HTT, vanishing above 370 °C (Figure 3). All these findings indicated that, below 400 °C, pyrolysis primarily caused the loss of the oxygen-rich cellulose and hemicellulose components through elimination reactions which give rise to unsaturated bonds and methylene carbons. It must be noted that only small amounts of carbonyl and carboxyl groups, which are expected to form in the pyrolysis of carbohydrates, were observed both in IR and NMR spectra. Moreover, the contribution of these functional groups decreased with increasing HTT above 300 °C, indicating that decarbonylation and decarboxylation reactions with loss of CO and CO_2 take place at relatively low temperatures, as reported in the literature [51]. The amount of aliphatic structures tended to increase upon heating at 370 °C, as highlighted both by the increased relative intensity in the 3000-2700 cm^{-1} region of IR spectra and in the 0-45 ppm region of the NMR spectra. Indeed, alkyl groups are expected to form from the reduction of alkoxy groups [43,44]. Upon further heating, the signals of aliphatic groups rapidly disappeared due to the loss of alkyl chains and the conversion of hydroaromatic methylene structures to aromatic ones.

Several indicators were used to characterize the aromaticity of chars. The aromaticity index, calculated from the H/C ratios previously determined [9], normalized and corrected in order to have a value of 1 for the highest degree of aromatization, according to Wiedemeier et al. [22], and here indicated as $H\text{-}C_{index}$, showed a steady increase with HTT (Figure 6a). The aromaticity index, AI_{MIR}, obtained from the ratio of the integrated areas in the 1650-1520 cm^{-1} (aromatic C=C ring stretching) and 3000-2800 cm^{-1} (aliphatic CHx stretching)

spectral regions, indicated that char aromaticity increased with HTT up to 700 °C for both feedstocks (Figure 6b). The decrease in AI_{MIR} observed for HTT ≈ 800 °C is, most probably, not indicative of a decrease in aromaticity, but rather to the formation of condensed polyaromatic structures. This process is highlighted by the trend of the aromatic C-H out-of-plane deformations in the 900-700 cm^{-1} region of IR spectra with increasing HTT. The aromaticity index obtained from the NMR spectra (AI_{NMR} in Figure 6c) indicates that the chars were practically fully aromatic structures for HTT > 400 °C. Moreover, as HTT further increased, the phenolic carbon signals (140-160 ppm) and the peak attributable to aromatic carbons ortho and para to oxygen-substituted carbons (120 ppm), tended to disappear. This trend can be associated to the formation of aromatic structures less substituted by OH and methoxyl groups. In agreement with the decrease in aromatic substitution, the IR band due to the aromatic CH stretching (at 3060 cm^{-1}) showed an increase in intensity with increasing HTT (Figure 1).

Additional evidence of the aromatization process came from the BPCA analysis, through the AI_{BPCA} indicator determined from total BPCA amount per organic carbon [22], reported in Figure 6d. The largest increase in AI_{BPCA} occurred for HTT between 235 and 420 °C, AI_{BPCA} reaching a plateau for higher HTT values.

Analogously to what was found in previous studies [22,52], AI_{NMR} and AI_{BPCA} were in good agreement throughout the HTT range examined, and showed the attainment of the maximum degree of aromaticity at approximately 400 °C, notwithstanding the different types of feedstock. The different trend of $H\text{-}C_{index}$ at the higher HTT values is ascribable to the fact that this index is strongly affected by condensation, this process too causing loss of H. As also found by Wiedemeier et al. [22], AI_{MIR} deviated from the aromaticity index obtained by NMR and BPCA.

Clear evidence of aromatic condensation processes is given by the ratio of B6CA to total BPCA [22], although there may be quantitativity issues at high temperatures since highly condensed aromatic structures may not be completely converted to quantifiable BPCAs. In our case, an increase in the proportion of B6CA biomarker was particularly evident in biochars prepared above 400 °C, the proportion of B6CA increasing with HTT, and becoming predominant above 600 °C (Figure 5). The aromatic condensation process was also suggested by the decrease in the aromatic C-H deformation signals with respect to the C=C ones in the IR spectra (Figure

2), with an intensity ratio decreasing by a factor of 3 by increasing HTT from ~ 600 °C to ~ 800 °C. Further evidence of condensation comes from EPR spectra (Figure 4), where unpaired electrons in progressively more condensed aromatic structures were clearly observed by increasing the pyrolysis temperature, ultimately giving rise to the electron conductive char obtained from carbonization of corncob at 800 °C. The EPR signal broadening observed for chars obtained by slow pyrolysis at the highest HTT values and by flash carbonization suggested the formation of a porous structure where oxygen can penetrate and interact with the aromatic radicals. On the basis of the literature, the line broadening of signals in EPR spectra of chars can be ascribed to dipolar interactions of the paramagnetic species present on the char surface with air, oxygen and moisture [47,48,49,53,54,55]. It is worthy of note that the line broadening was observed for those samples that have been found to have a higher specific surface area in a previous work [9].

The degree of condensation of the aromatic structures was estimated by applying the rectangle-like model proposed by Xiao et al. [23] to H/C and BPCA data obtained for HTT ≥ 369 °C. The average cluster size, reported in Table 3, remained 4×4 for HTT < 500 °C and then increased up to 14×14 at the highest HTT.

As far as the differences between corncob and *Miscanthus* are concerned, IR spectroscopy highlighted a higher loss of aliphatic ether and alcohol functionalities for corncob at the lower HTT values. Moreover, for corncob, aromatic C-O and phenolic groups persisted at higher temperatures. This is probably to be ascribed to the fact that *Miscanthus* is typically composed of cellulose, hemicellulose and lignin in the weight ratios 4.2:2.1:1 [56], whereas corncob has a significantly higher hemicellulose content, the ratios being 3.2:3.7:1 [57]. Investigation of hemicellulose, cellulose and lignin pyrolysis behavior [51] has shown that the thermal decomposition of hemicellulose occurs mostly at temperatures below 315 °C, that of cellulose occurs at temperatures between 315 and 400 °C, while lignin thermally decomposes very slowly over the whole pyrolysis temperature range considered here. Moreover, the pyrolysis reactions of hemicellulose and lignin are exothermic, whereas that of cellulose is endothermic [51]. These general behaviors were confirmed for our samples by thermogravimetric analyses (Figure S.1). A consequence of the different thermal properties of lignin, hemicellulose and cellulose pyrolysis reactions is that, at a set temperature of 250 °C, the actual pyrolysis temperature for corncob is significantly higher than that for *Miscanthus*, as reported in a previous

study [9]. On the other hand, at set pyrolysis temperatures of 300 and 350 °C, *Miscanthus* reached a slightly higher temperature compared to corncob. In this temperature range, thermal decomposition occurs for both cellulose and lignin, suggesting that the higher lignin content of *Miscanthus* is likely responsible for the higher HTT reached in the retort.

When comparing the aromatic structures for chars obtained from the two feedstocks, IR spectroscopy suggested a lower degree of substitution for the aromatic rings in *Miscanthus*, in agreement with the NMR results at 416 °C. On the other hand, no significant differences in aromatic cluster size were found by BPCA analysis. This apparent discrepancy could be simply explained assuming a different architecture of the condensed aromatic structures.

As far as the type of process is concerned, the char obtained from corncob through flash carbonization had aromaticity similar to that observed for chars obtained from slow pyrolysis at lower temperatures but a higher degree of aromatic condensation. This difference is likely related to secondary carbon formation processes favoured by the higher chamber pressure and the air flow direction opposite to the flame front in flash carbonization [26].

5. Conclusions

The combined use of several complementary techniques allowed a detailed picture of the sequence of transformation processes from biomass to chars to be obtained. The use of a multi-method approach is extremely important given the intrinsic limitations of each method. As observed by others [58], the major steps of the pyrolytic process of biomass materials are dehydration, carbonyl group formation and elimination, the decomposition of aliphatic units and the formation of aromatic ones, which, eventually, form condensed aromatic sheets giving rise to micrographitic domains. IR and NMR spectroscopies gave evidence of the thermal decomposition of cellulose and lignin and of the formation of aromatic structures with increasing condensation degree as the temperature is increased. The type of biomass does not affect the degree of aromatic condensation of the solid residues that are formed upon pyrolysis at high temperatures, but influences the architecture of the aromatic condensed systems. Larger differences are observed at the lower temperatures due to the different proportions of cellulose, hemicellulose and lignin in the feedstocks.

Acknowledgments

The authors would like to thank Morten Grønli and Liang Wang (Norwegian University of Science and Technology) and the late Michael Antal Jr. (Hawaii Natural Energy Institute) for providing charred materials for this study. The authors also thank Lauric Cécillon (Université Grenoble Alpes) for providing R script for correction of IR spectra and Dr. Calogero Pinzino (ICCOM-CNR) for performing EPR experiments. Funding for this research was provided by the Research Council of Norway through the project NFR 195731 "Advanced Techniques to Evaluate the Long-term Stability and Carbon Sequestration Potential of Different Types of Biochar", NFR197531 and by NFR supported NIBIO SIS-Jordkarbon project.

References

[1] B. Glaser, J. Lehmann, W. Zech, Ameliorating physical and chemical properties of highly weathered soils in the tropics with charcoal - a review, Biology and Fertility of Soils 35(4) (2002) 219-230.

[2] S. Nanda, A.K. Dalai, F. Berruti, J.A. Kozinski, Biochar as an exceptional bioresource for energy, agronomy, carbon sequestration, activated carbon and specialty materials, Waste and Biomass Valorization 7(2) (2016) 201-235.

[3] J.S. Cha, S.H. Park, S.C. Jung, C. Ryu, J.K. Jeon, M.C. Shin, Y.K. Park, Production and utilization of biochar: a review, Journal of Industrial and Engineering Chemistry 40 (2016) 1-15

[4] S. Meyer, B. Glaser, P. Quicker, Technical, economical, and climate-related aspects of biochar production technologies: a literature review, Environmental Science & Technology 45(22) (2011) 9473-9483.

[5] M. Keiluweit, P.S. Nico, M.G. Johnson, M. Kleber, Dynamic molecular structure of plant biomass-derived black carbon (biochar), Environmental Science & Technology 44(4) (2010) 1247-1253.

[6] S. Kloss, F. Zehetner, A. Dellantonio, R. Hamid, F. Ottner, V. Liedtke, M. Schwanninger, M.H. Gerzabek, G. Soja, Characterization of slow pyrolysis biochars: effects of feedstocks and pyrolysis temperature on biochar properties, Journal of Environmental Quality 41(4) (2012) 990-1000.

[7] M.J. Antal, M. Grønli, The art, science, and technology of charcoal production, Industrial & Engineering Chemistry Research 42(8) (2003) 1619-1640.

[8] H. Zhang, R.P. Voroney, G.W. Price, Effects of temperature and processing conditions on biochar chemical properties and their influence on soil C and N transformations, Soil Biology and Biochemistry 83 (2015) 19-28.

[9] A. Budai, L. Wang, M. Grønli, L.T. Strand, M.J. Antal, S. Abiven, A. Dieguez-Alonso, A. Anca-Couce, D.P. Rasse, Surface properties and chemical composition of corncob and Miscanthus biochars: effects of production temperature and method, Journal of Agricultural and Food Chemistry 62(17) (2014) 3791-3799.

[10] Y. Kuzyakov, I. Bogomolova, B. Glaser, Biochar stability in soil: Decomposition during eight years and transformation as assessed by compound-specific ^{14}C analysis, Soil Biology and Biochemistry 70 (2014) 229-236.

[11] M.W.I. Schmidt, A.G. Noack, Black carbon in soils and sediments: analysis, distribution, implications, and current challenges, Global Biogeochemical Cycles 14(3) (2000) 777-793.

[12] L. Luo, C. Xu, Z. Chen, S. Zhang, Properties of biomass-derived biochars: combined effects of operating conditions and biomass types, Bioresource Technology 192 (2015) 83-89.

[13] X. Cao, J.J. Pignatello, Y. Li, C. Lattao, M.A. Chappell, N. Chen, L.F. Miller, J. Mao, Characterization of wood chars produced at different temperatures using advanced solid-state ^{13}C NMR spectroscopic techniques, Energy & Fuels 26(9) (2012) 5983-5991.

[14] P. Conte, G. Alonzo, Environmental NMR: fast-field-cycling relaxometry, eMagRes 2 (2013) 389-398.

[15] J. Kaal, M.P.W. Schneider, M.W.I. Schmidt, Rapid molecular screening of black carbon (biochar) thermosequences obtained from chestnut wood and rice straw: a pyrolysis-GC/MS study, Biomass & Bioenergy 45 (2012) 115-129.

[16] D.B. Wiedemeier, S.Q. Lang, M. Gierga, S. Abiven, S.M. Bernasconi, G.L. Früh-Green, I. Hajdas, U.M. Hanke, M.D. Hilf, C.P. McIntyre, M.P.W. Scheider, R.H. Smittenberg, L. Wacker, G.L.B. Wiesenberg, M.W.I. Schmidt, Characterization, quantification and compound-specific isotopic analysis of pyrogenic carbon using benzene polycarboxylic acids (BPCA), Journal of Visualized Experiments (111) (2016) e53922.

[17] N. Baccile, G. Laurent, F. Babonneau, F. Fayon, M.-M. Titirici, M. Antonietti, Structural characterization of hydrothermal carbon spheres by advanced solid-state MAS 13C NMR Investigations, The Journal of Physical Chemistry C 113(22) (2009) 9644-9654.

[18] M. Bardet, S. Hediger, G. Gerbaud, S. Gambarelli, J.F. Jacquot, M.F. Foray, A. Gadelle, Investigation with 13C NMR, EPR and magnetic susceptibility measurements of char residues obtained by pyrolysis of biomass, Fuel 86(12–13) (2007) 1966-1976.

[19] C.E. Brewer, K. Schmidt-Rohr, J.A. Satrio, R.C. Brown, Characterization of biochar from fast pyrolysis and gasification systems, Environmental Progress & Sustainable Energy 28(3) (2009) 386-396.

[20] X. Cao, K.S. Ro, M. Chappell, Y. Li, J. Mao, Chemical structures of swine-manure chars produced under different carbonization conditions investigated by advanced solid-state ^{13}C Nuclear Magnetic Resonance (NMR) spectroscopy, Energy & Fuels 25(1) (2011) 388-397.

[21] C. Falco, F. Perez Caballero, F. Babonneau, C. Gervais, G. Laurent, M.-M. Titirici, N. Baccile, Hydrothermal carbon from biomass: structural differences between hydrothermal and pyrolyzed carbons via ^{13}C solid state NMR, Langmuir 27(23) (2011) 14460-14471.

[22] D.B. Wiedemeier, S. Abiven, W. C. Hockaday, M. Keiluweit, M. Kleber, C.A. Masiello, A.V. McBeath, P.S. Nico, L.A. Pyle, M.P.W. Schneider, R.J. Smernik, G.L.B. Wiesenberg, M.W.I. Schmidt, Aromaticity and degree of aromatic condensation of char, Organic Geochemistry 78 (2015) 135-143.

[23] X. Xiao, Z. Chen, B. Chen, H/C atomic ratio as a smart linkage between pyrolytic temperatures, aromatic clusters and sorption properties of biochars derived from diverse precursory materials, Scientific Reports 6 (2016) 22644.

[24] S. Brodowski, A. Rodionov, L. Haumaier, B. Glaser, W. Amelung, Revised black carbon assessment using benzene polycarboxylic acids, Organic Geochemistry 36(9) (2005) 1299-1310.

[25] B. Glaser, L. Haumaier, G. Guggenberger, W. Zech, Black carbon in soils: the use of benzenecarboxylic acids as specific markers, Organic Geochemistry 29(4) (1998) 811-819.

[26] M.J. Antal, K. Mochidzuki, L.S. Paredes, Flash carbonization of biomass, Industrial & Engineering Chemistry Research 42(16) (2003) 3690-3699.

[27] T.G. Bloemberg, J. Gerretzen, H.J.P. Wouters, J. Gloerich, M. van Dael, H.J.C.T. Wessels, L.P. van den Heuvel, P.H.C. Eilers, L.M.C. Buydens, R. Wehrens, Improved parametric time warping for proteomics, Chemometrics and Intelligent Laboratory Systems 104(1) (2010) 65-74.

[28] R. Wehrens, T.G. Bloemberg, P.H.C. Eilers, Fast parametric warping of peak lists, Bioinformatics 31(18) (2015) 3063-3065.

[29] Y. Guo, R.M. Bustin, FTIR spectroscopy and reflectance of modern charcoals and fungal decayed woods: implications for studies of inertinite in coals, International Journal of Coal Geology 37(1–2) (1998) 29-53.

[30] M. Geppi, C. Forte, The SPORT-NMR software: a tool for determining relaxation times in unresolved NMR spectra, Journal of Magnetic Resonance 137(1) (1999) 177-185.

[31] C.M. Preston, J.A. Trofymow, J. Niu, C.A. Fyfe, ^{13}CPMAS-NMR spectroscopy and chemical analysis of coarse woody debris in coastal forests of Vancouver Island, Forest Ecology and Management 111 (1998) 51-68.

[32] C.P. Poole, Electron Spin Resonance. A Comprehensive Treatise on Experimental Techniques. in: Electron Spin Resonance. A Comprehensive Treatise on Experimental Techniques, Wiley, New York, 1967.

[33] D.B. Wiedemeier, M.D. Hilf, R.H. Smittenberg, S.G. Haberle, M.W.I. Schmidt, Improved assessment of pyrogenic carbon quantity and quality in environmental samples by high-performance liquid chromatography, Journal of Chromatography A 1304 (2013) 246-250.

[34] M.P.W. Schneider, R. H. Smittenberg, T. Dittmar, M.W.I. Schmidt, Comparison of gas with liquid chromatography for the determination of benzene polycarboxylic acids as molecular tracers of black carbon, Organic Geochemistry 42 (2011) 275-282.

[35] M. Poletto, A.J. Zattera, R.M.C. Santana, Structural differences between wood species: Evidence from chemical composition, FTIR spectroscopy, and thermogravimetric analysis, Journal of Applied Polymer Science 126(S1) (2012) E337-E344.

[36] J. Ibarra, E. Muñoz, R. Moliner, FTIR study of the evolution of coal structure during the coalification process, Organic Geochemistry 24(6–7) (1996) 725-735.

[37] J.C.C. Freitas, T.J. Bonagamba, F.G. Emmerich, Investigation of biomass- and polymer-based carbon materials using ^{13}C high-resolution solid-state NMR, Carbon 39(4) (2001) 535-545.

[38] I. Pastorova, R.E. Botto, P.W. Arisz, J.J. Boon, Cellulose char structure: a combined analytical Py-GC-MS, FTIR, and NMR study, Carbohydrate Research 262(1) (1994) 27-47.

[39] R.H. Atalla, D.L. VanderHart, The role of solid state ^{13}C NMR spectroscopy in studies of the nature of native celluloses, Solid State Nuclear Magnetic Resonance 15(1) (1999) 1-19.

[40] W. Kolodziejski, J.S. Frye, G.E. Maciel, Carbon-13 nuclear magnetic resonance spectrometry with cross polarization and magic-angle spinning for analysis of lodgepole pine wood, Analytical Chemistry 54(8) (1982) 1419-1424.

[41] J. Mao, K.M. Holtman, J.T. Scott, J.F. Kadla, K. Schmidt-Rohr, Differences between lignin in unprocessed wood, milled wood, mutant wood, and extracted lignin detected by 13C solid-state NMR, Journal of Agricultural and Food Chemistry 54(26) (2006) 9677-9686.

[42] L. Calucci, D.P. Rasse, C. Forte, Solid-state Nuclear Magnetic Resonance characterization of chars obtained from hydrothermal carbonization of corncob and Miscanthus, Energy & Fuels 27(1) (2013) 303-309.

[43] S.C. Teerman, R.J. Hwang, Evaluation of the liquid hydrocarbon potential of coal by artificial maturation techniques, Organic Geochemistry 17(6) (1991) 749-764.

[44] J. Zawadzki, M. Wisniewski, 13C NMR study of cellulose thermal treatment, Journal of Analytical and Applied Pyrolysis 62(1) (2002) 111-121.

[45] C.M. Preston, Carbon-13 solid-state NMR of soil organic matter - using the technique effectively, Canadian Journal of Soil Science 81(3) (2001) 255-270.

[46] J.A. Baldock, R.J. Smernik, Chemical composition and bioavailability of thermally, altered Pinus resinosa (Red Pine) wood, Organic Geochemistry 33(9) (2002) 1093-1109.

[47] J.-W. Feng, S. Zheng, G.E. Maciel, EPR Investigations of the effects of inorganic additives on the charring and char/air interactions of cellulose, Energy & Fuels 18(4) (2004) 1049-1065.

[48] S.J. Boyer, R.B. Clarkson, Electron paramagnetic resonance studies of an active carbon: the influence of preparation procedure on the oxygen response of the linewidth, Colloids and Surfaces A: Physicochemical and Engineering Aspects 82(3) (1994) 217-224.

[49] A.A. Konchits, B.D. Shanina, M.Y. Valakh, I.B. Yanchuk, V.O. Yukhymchuk, A.D. Alexeev, T.A. Vasilenko, A.N. Molchanov, A.K. Kirillov, Local structure, paramagnetic properties, and porosity of natural coals: spectroscopic studies, Journal of Applied Physics 112(4) (2012) 043504.

[50] K. Hammes, R.J. Smernik, J.O. Skjemstad, A. Herzog, U.F. Vogt, M.W.I. Schmidt, Synthesis and characterisation of laboratory-charred grass straw (Oryza saliva) and chestnut wood (Castanea sativa) as reference materials for black carbon quantification, Organic Geochemistry 37(11) (2006) 1629-1633.

[51] H. Yang, R. Yan, H. Chen, D.H. Lee, C. Zheng, Characteristics of hemicellulose, cellulose and lignin pyrolysis, Fuel 86(12–13) (2007) 1781-1788.

[52] A.V. McBeath, R.J. Smernik, M.P.W. Schneider, M.W.I. Schmidt, E.L. Plant, Determination of the aromaticity and the degree of aromatic condensation of a thermosequence of wood charcoal using NMR, Organic Geochemistry 42(10) (2011) 1194-1202.

[53] J.W. Armstrong, C. Jackson, H. Marsh, Electron spin resonance in carbonized organic polymers—II. Effects of adsorbed oxygen, Carbon 2(3) (1964) 239-252.

[54] V.A. Atsarkin, V.V. Demidov, G.A. Vasneva, F.S. Dzheparov, P.J. Ceroke, B.M. Odintsov, R.B. Clarkson, Mechanism of oxygen response in carbon-based sensors, Journal of Magnetic Resonance 149(1) (2001) 85-89.

[55] O.Y. Grinberg, B.B. Williams, A.E. Ruuge, S.A. Grinberg, D.E. Wilcox, H.M. Swartz, J.H. Freed, Oxygen effects on the EPR signals from wood charcoals: experimental results and the development of a model, The Journal of Physical Chemistry B 111(46) (2007) 13316-13324.

[56] N. Brosse, A. Dufour, X. Meng, Q. Sun, A.Ragauskas, Miscanthus: a fast-growing crop for biofuels and chemicals production, Biofuels, Bioproducts and Biorefining 6(5) (2012) 580-598.

[57] M. Pointner, P. Kuttner, T. Obrlik, A. Jäger, H. Kahr, Composition of corncobs as a substrate for fermentation of biofuels, Agronomy Research 12(2) (2014) 391-396.

[58] R.K. Sharma, J.B. Wooten, V.L. Baliga, X. Lin, W. Geoffrey Chan, M.R. Hajaligol, Characterization of chars from pyrolysis of lignin, Fuel 83(11–12) (2004) 1469-1482.

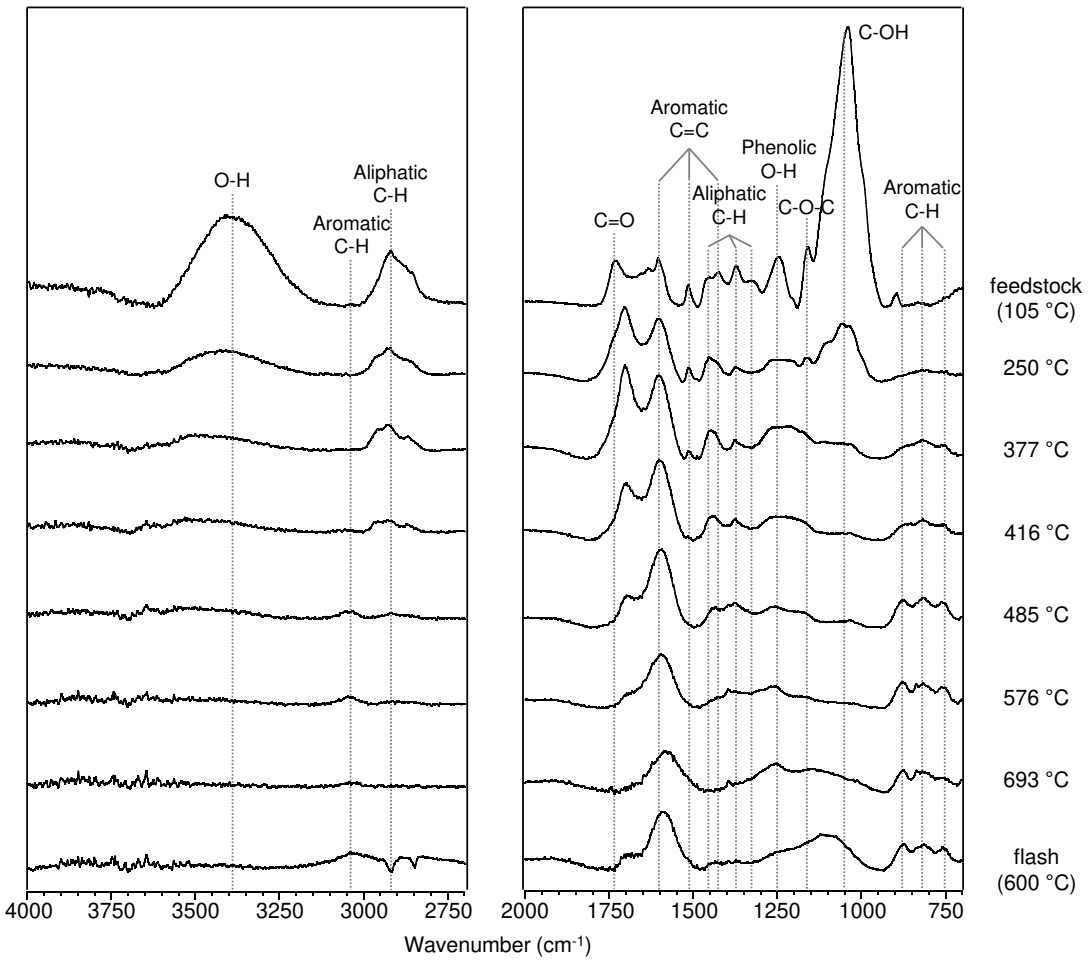

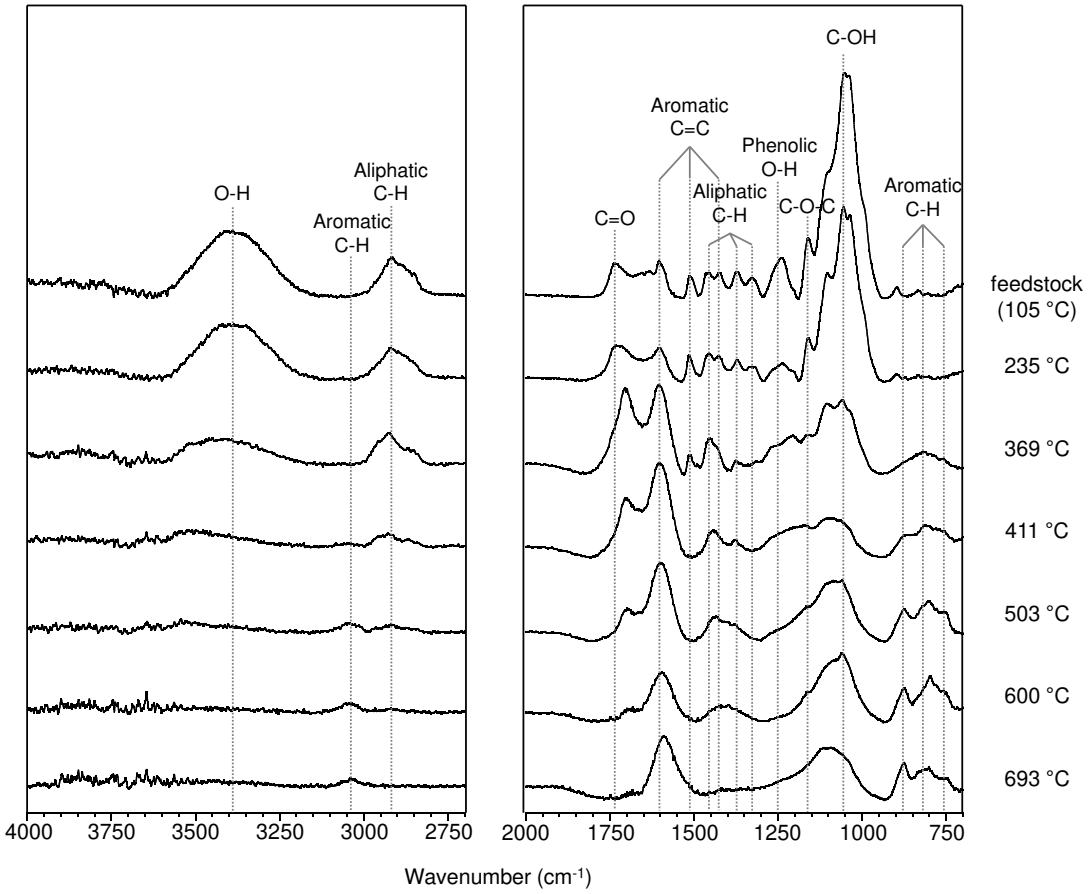

Figure 1. IR spectra of (top) corncob and (bottom) *Miscanthus* feedstocks (after drying at 105 °C) and chars obtained from slow pyrolysis with different HTT values (in degrees centigrade, indicated) and flash carbonization (for corncob only).

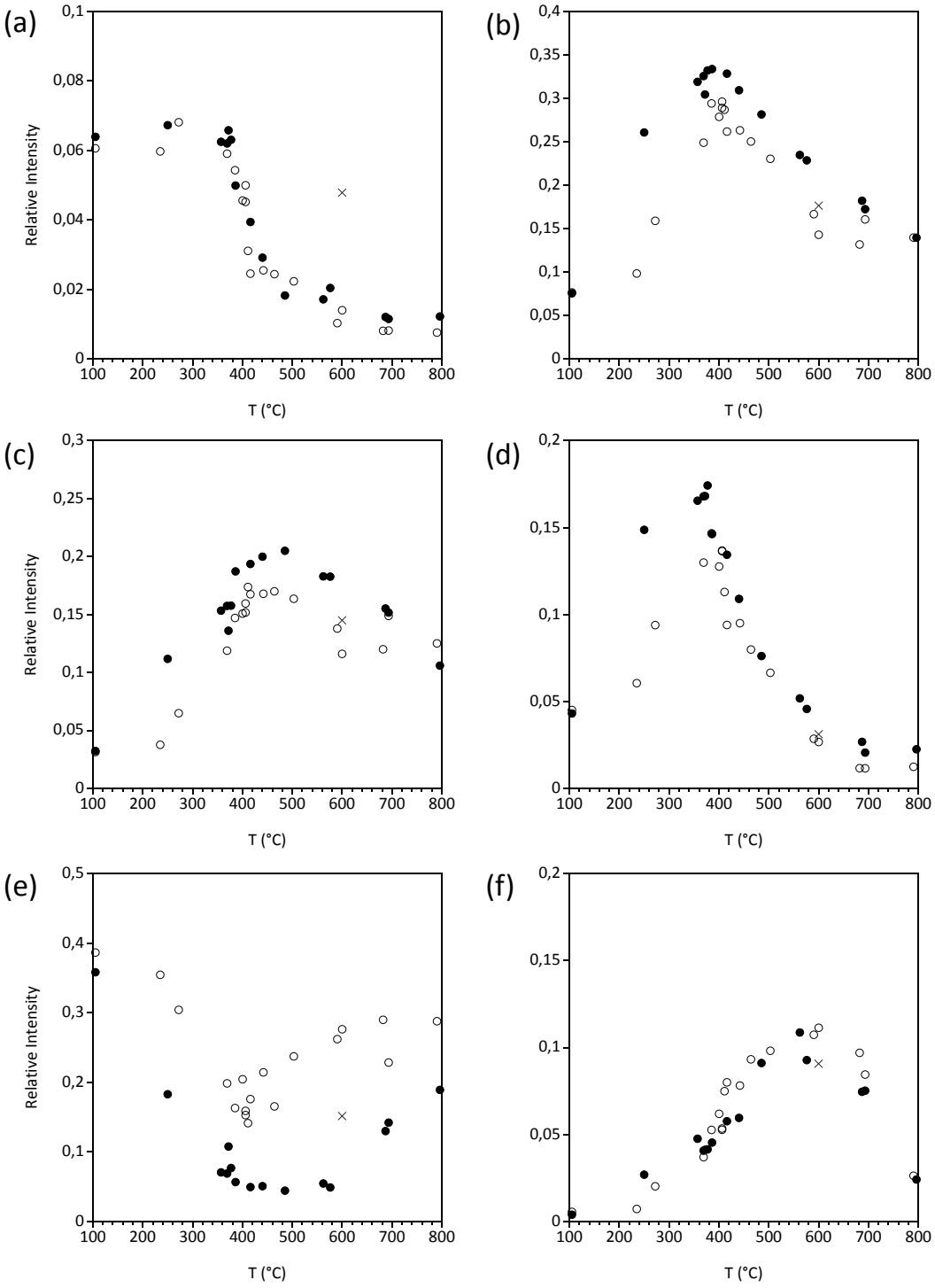

Figure 2. Relative contribution to IR spectra of (a) saturated, (b) unsaturated, (c) aromatic C=C, (d) C=O, (e) O-alkyl and (f) aromatic CH bands for (●) corncob and (○) *Miscanthus* feedstocks and chars obtained from slow pyrolysis with different HTT values, and for (×) corncob char obtained from flash carbonization. The spectral regions are as defined in section 2.2. T is the HTT or process temperature for chars, whereas it is the temperature used in sample preparation for feedstocks.

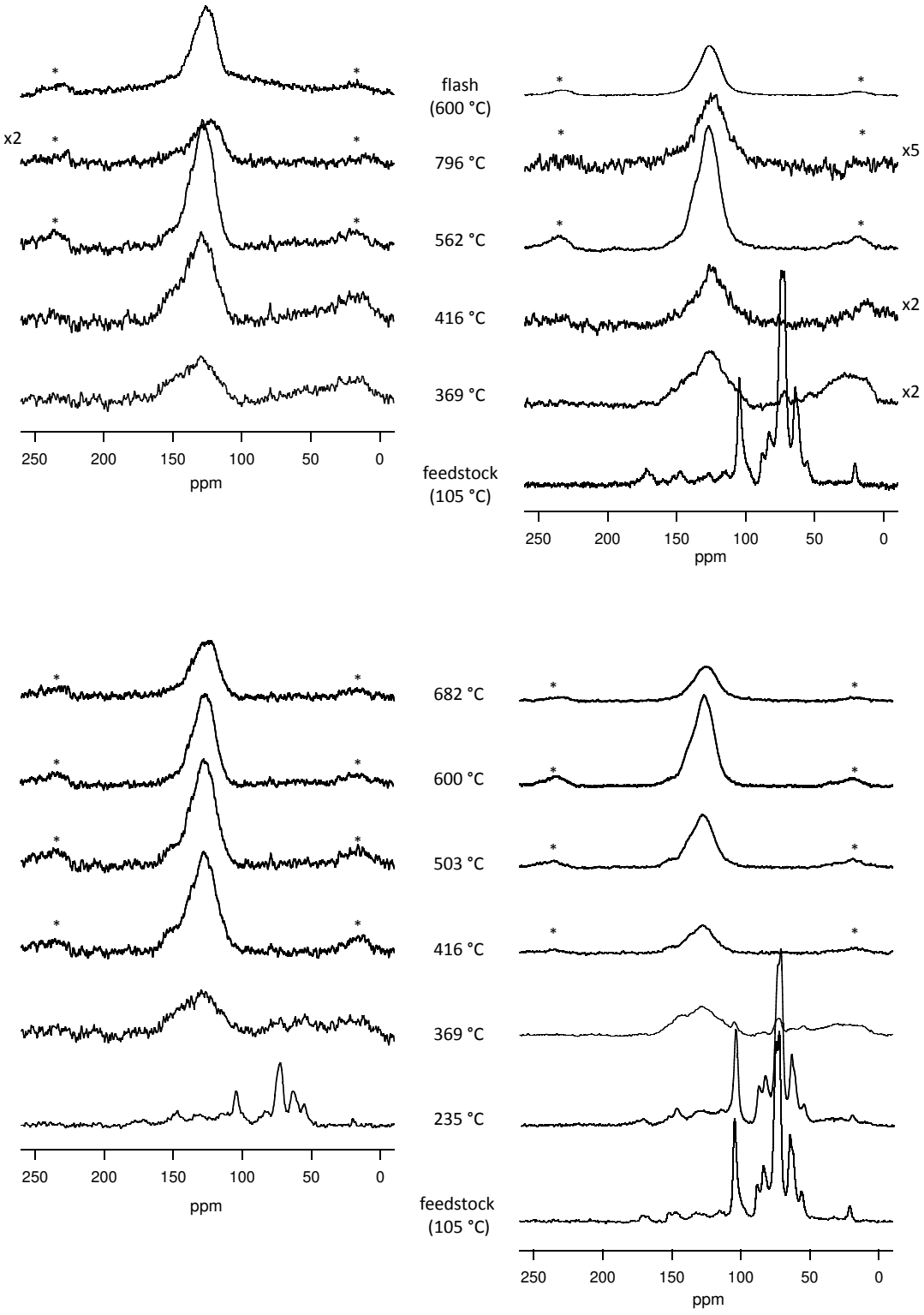

Figure 3. ^{13}C DE-MAS (left) and CP-MAS (right) NMR spectra of corncob (top) and *Miscanthus* (bottom) feedstocks (after drying at 105 °C) and char samples obtained from slow pyrolysis at the indicated temperatures and, in the case of corncob, also from flash carbonization. The spectra of the feedstocks have

been reported previously [42]. Asterisks denote spinning sidebands. The broad signal detectable at the base of the aromatic peak in the DE-MAS spectrum of the flash carbonized corncob is a background signal due to the rotor.

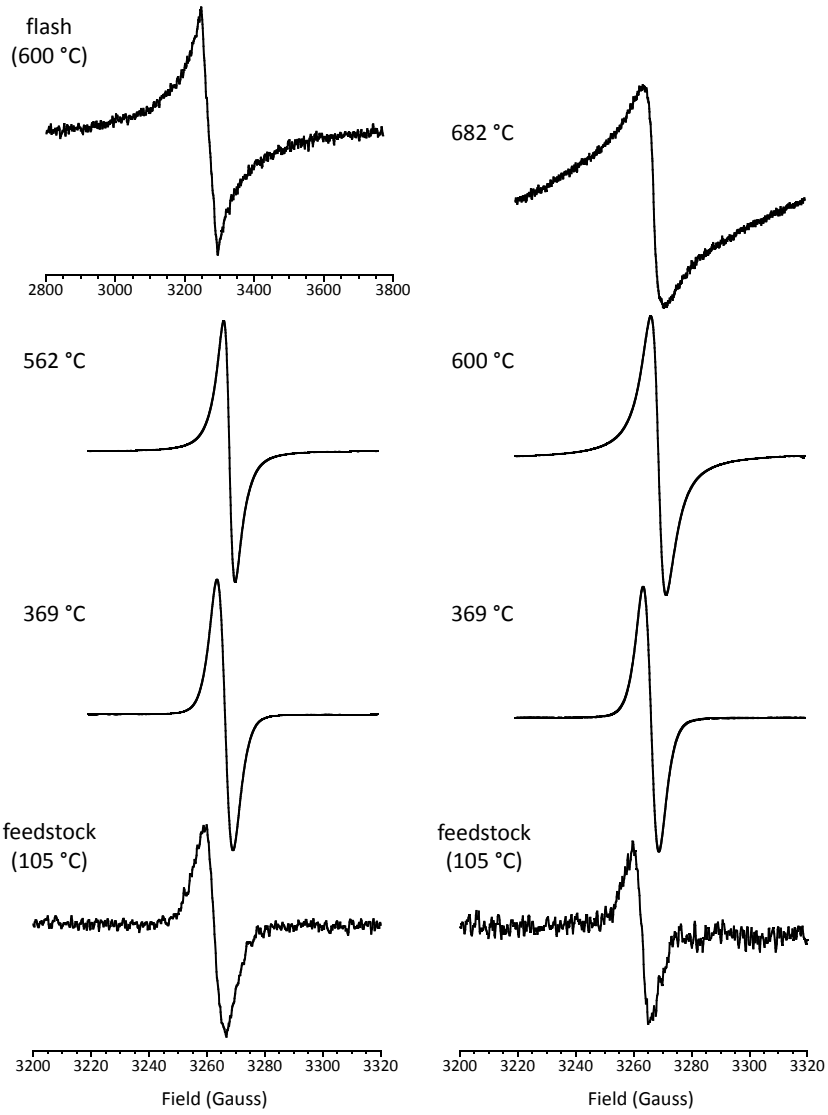

Figure 4. Representative EPR spectra of corncob (left) and *Miscanthus* (right) feedstock (after drying at 105 °C) and char samples obtained from slow pyrolysis at the indicated HTT values and from flash carbonization (for corncob).

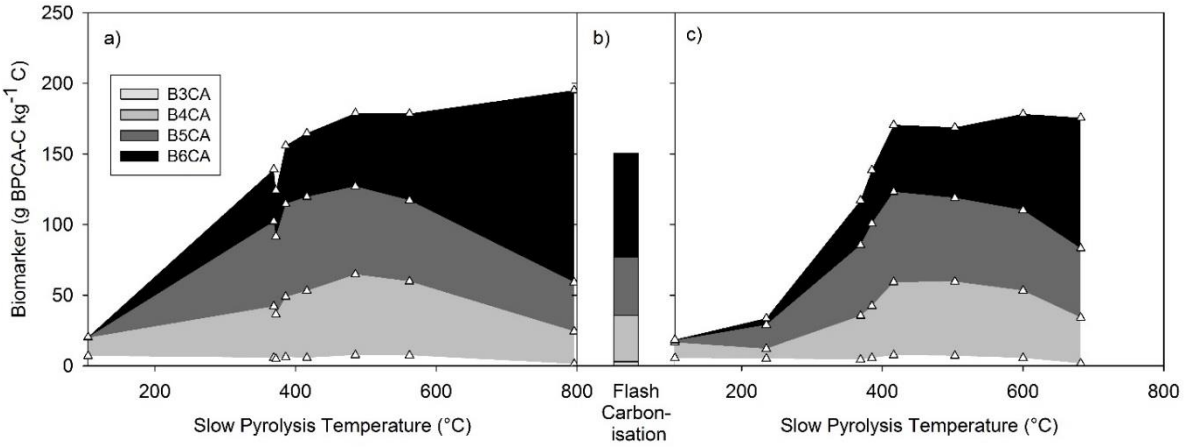

Figure 5. Relative BPCA-C content and distribution of B3CA, B4CA, B5CA and B6CA for (a) corncob feedstock and chars obtained by slow pyrolysis at different HTT, (b) corncob char produced by flash carbonization, and (c) *Miscanthus* feedstock and chars obtained by slow pyrolysis at different HTT.

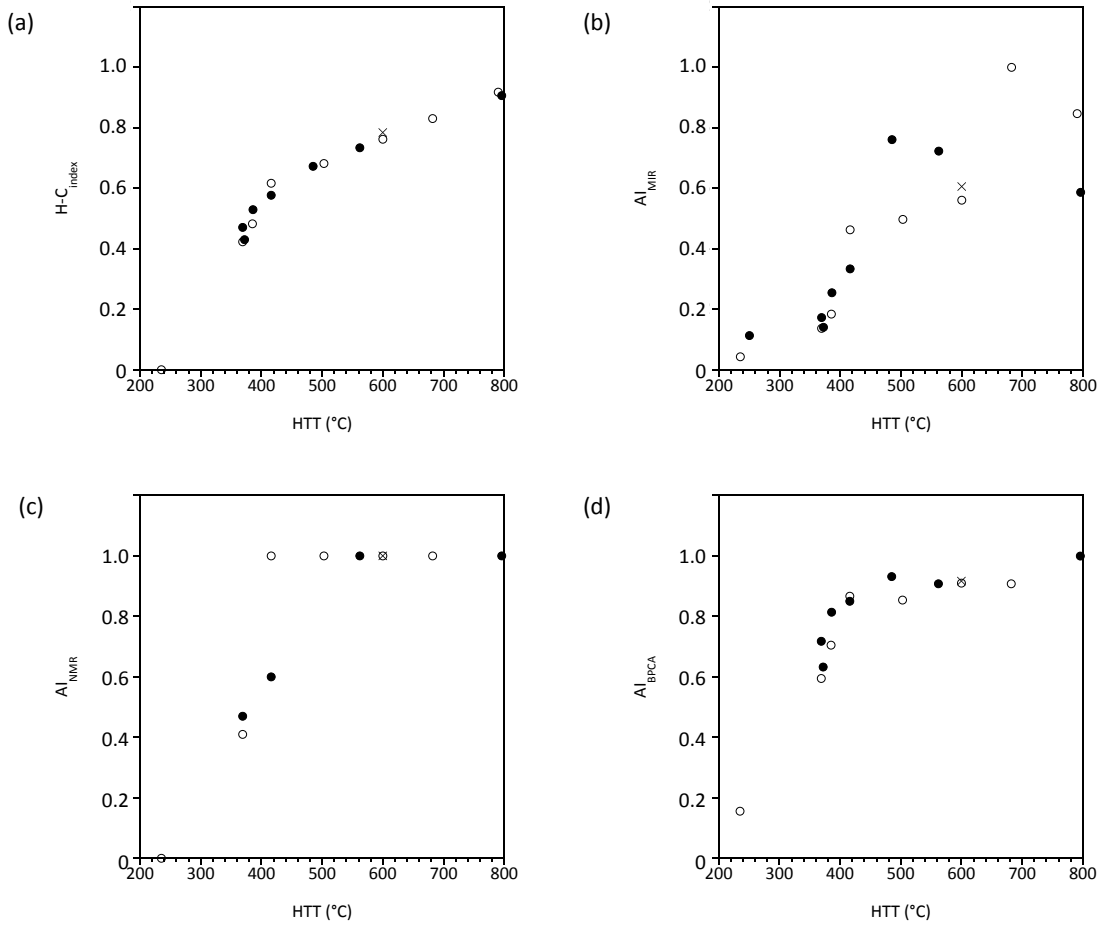

Figure 6. Aromaticity index obtained from (a) H/C elemental ratios, (b) IR spectra, (c) ^{13}C DE-MAS NMR spectra, and (d) BPCA analyses for (●) corncob and (○) *Miscanthus* chars obtained from slow pyrolysis with different HTT values, and for (×) corncob char obtained from flash pyrolysis.

Table 1. Overall relative signal intensities, normalized with respect to the sample weight, observed in the ^{13}C DE-MAS spectra for the different samples and distribution of components (%). Errors are within 5 %.

Sample	T (°C)	intensity	Alkyl C	Carbohydrate C	Lignin C	Aromatic C	Carboxyl C	Carbonyl C	Acetate
Corncob	369	1.89	24		23	47	4	2	
	416	2.44	17	1	17	60	3	2	
	562	3.03				100			
	796	1.00[a]				100			
	Flash					100			
Miscanthus	235	0.81		48	47		3		2
	369	1.64	12	3	38	41	3	3	
	416	1.83				100			
	503	2.36				100			
	600	2.05				100			
	682	1.23				100			

Table 2. Values of *g*, peak-to-peak linewidth (ΔHpp) and relative contribution for Lorentzian and Gaussian lines in the EPR spectra of *Miscanthus* and corncob feedstocks (FS) and chars obtained from slow pyrolysis at the indicated HTT values. The radical concentration corresponding to the total spectral intensity is given as spins/g.

Feedstock	**Sample**	**Lorentzian**			**Gaussian**			**Spins/g**
		g	**weight %**	**ΔHpp (G)**	***g***	**weight %**	**ΔHpp (G)**	
Corncob	FS	2.0046	100	7.2				$(4.8 \pm 0.1)\ 10^{16}$
	369 °C	2.0030	46	3.8	2.0033	54	7.1	$(1.3 \pm 0.1)\ 10^{19}$
	416 °C	2.0029	60	4.4	2.0033	40	7.6	$(3.9 \pm 0.2)\ 10^{19}$
	562 °C	2.0024	94	4.2	2.0033	6	15	$(9.2 \pm 0.3)\ 10^{19}$
Miscanthus	FS	2.0044	100	6.5				$(2.6 \pm 0.1)\ 10^{16}$
	235 °C	2.0032	56	4.1	2.0034	44	8.5	$(2.0 \pm 0.1)\ 10^{17}$
	369 °C	2.0032	46	3.7	2.0034	54	7.1	$(8.6 \pm 0.2)\ 10^{18}$
	416 °C	2.0026	65	4.2	2.0028	35	7.8	$(6.9 \pm 0.2)\ 10^{19}$
	503 °C	2.0025	79	4.3	2.0023	21	8.1	$(8.3 \pm 0.2)\ 10^{19}$
	600 °C	2.0025	78	5.5	2.0023	22	24	$(8.5 \pm 0.2)\ 10^{19}$
	682 °C	2.0027	26	7	2.0021	74	34	$(4.3 \pm 0.1)\ 10^{19}$

Table 3. Cluster size estimated from H/C atomic ratios and BPCAs. Cluster size is given as the number n of aromatic rings along one side of an n×n cluster [23].

Sample	T (°C)	cluster size n	
		H/C	B6CA/BPCA
Corncob	377	2	4
	416	2	4
	485	3	4
	576	4	5
	796	14	12
	Flash	5	7
Miscanthus	369	2	4
	385	2	4
	411	3	4
	503	3	4
	600	5	5
	682	7	7